Published in : Journal of Magnetism and Magnetic Materials (2020), vol. 505, 166725
DOI:10.1016/j.jmmm.2020.166725
Status : Postprint (Author's version)

Ni-substitution effect on the properties of $Ba_{0.5}Sr_{1.5}Zn_{2-x}Ni_xFe_{12}O_{22}$ powders

Tatyana Koutzarova[a], Svetoslav Kolev[a], Kiril Krezhov[a], Borislava Georgieva[a,*], Chavdar Ghelev[a], Daniela Kovacheva[b], Benedicte Vertruyen[c], Raphael Closset[c], Lan Maria Tran[d], Michal Babij[d], Andrzej J. Zaleski[d]

[a] *Institute of Electronics, Bulgarian Academy of Sciences, 72 Tsarigradsko Chaussee, 1784 Sofia, Bulgaria*
[b] *Institute of General and Inorganic Chemistry, Bulgarian Academy of Sciences, Acad. Georgi Bonchev Str., bld. 11, 1113 Sofia, Bulgaria*
[c] *Greenmat, Chemistry Department, University of Liege, 11 allée du 6 août, 4000 Liège, Belgium*
[d] *Institute of Low Temperature and Structure Research, Polish Academy of Sciences, Ul. Okólna 2, 50-422 Wroclaw, Poland*
[*] *Corresponding author. E-mail address: b.georgiewa@abv.bg (B. Georgieva)*

KEYWORDS: Y-type hexaferrites, Sol–gel auto-combustion, Ni-substitution, *ac* susceptibility Magnetic properties, Magnetic phase transitions.

ABSTRACT

We consider the influence of the magnetic cation (Ni^{2+}) substitution on the structural and magnetic properties of $Ba_{0.5}Sr_{1.5}Zn_{2-x}Ni_xFe_{12}O_{22}$ (x = 0.8, 1, 1.5) powders. The powders were synthesized by using the citric-acid sol–gel auto-combustion method. Their *ac*-magnetization was measured in an ac-magnetic field with an amplitude of 10 Oe and a frequency of 1000 Hz to detect any magnetic phase transitions. A strong influence of the Ni-substitution on the magnetic properties was thus observed. A magnetic phase transition from a helicoidal to a ferrimagnetic spin order at 284 K was observed for the sample $Ba_{0.5}Sr_{1.5}Zn_{0.5}Ni_{1.5}Fe_{12}O_{22}$. The magnetic-phase transition from conical spin order to hellicoidal spin order was registered at 149 K and 177 K for x = 0.8 and x = 1, respectively. Triple hysteresis loops were observed for all samples at 4.2 K, which indicates the presence of two kinds of ferromagnetic states with different magnetization values.

Published in : Journal of Magnetism and Magnetic Materials (2020), vol. 505, 166725
DOI:10.1016/j.jmmm.2020.166725
Status : Postprint (Author's version)

1. Introduction

For the magneto-electric multiferroic materials to be suitable for practical applications, the magneto-electric coupling in them should be both large and active at room temperature, with the magnetic ordering temperature being high. Preparation of a material in which large ferroelectricity and strong ferromagnetism coexist would be a milestone for modern electrics and functionalized materials [1]. It is believed that the large magneto-electric effect is due to the possibility of a strong interplay between magnetization and electric polarization in insulating systems with long-wavelength cycloidal, sinusoidal, spiral and conical magnetic structures [2,3]. The hexaferrites are one class of materials with a long-wavelength magnetic structure [4,5], and are thus promising multiferroic materials possessing potential for manipulation of the polarization by a magnetic field up to room temperature [6–12]. The crystal structure of Y hexaferrites belongs to the rhombohedral space group R(-3 m) and can be considered as consisting of two types of crystal S- and T-blocks consecutively stacked along the hexagonal c axis in the sequence (TST'ST"S"), with the primes indicating rotation about the c axis by 120° [13]. The hexagonal unit cell is thus made up of three T-blocks and three S-blocks containing 18 oxygen layers. There are six sites for metals, four of them octahedral and two tetrahedral in the S-block ($Me_2Fe_4O_8$; spinel block). The T-block ($Ba_2Fe_8O_{14}$) is made up of four oxygen layers, with a barium atom substituting an oxygen atom in the inner two layers, which are opposite to one another in the neighboring layers, resulting in two tetrahedral and six octahedral sites [13]. All cations (Me^{+2} and Fe^{+3}) are positioned in six specific crystallographic sites: two tetrahedral sites and four octahedral sites. For example, the Zn^{2+} cations prefer to occupy tetrahedral sites, together with the Fe^{3+} cations in $Ba_{2-x}Sr_xZn_2Fe_{12}O_{22}$ [14,15]. Using the qualitative approach and magnetic data, [16] predicted the orientation of the magnetic moments in the Y-type ferrite sublattices and the relative strength of the super exchange interactions. Thus, for the Zn_2Y he evaluated the saturation magnetization value to be 20 μ_B if the zinc atoms are present only in the tetrahedral sites, but the value measured is only 17.6 μ_B. The two magnetic sublattices are different from the crystal structural blocks, namely, L_m and S_m blocks alternating along [0 0 1], which bear, correspondingly, opposite large and small magnetization [17]. Taking into consideration these two sublattices, L_m and S_m, helps one understand the magnetic structures of Y-type hexaferrites because the strongest magnetic interaction occurs inside the T block. The superexchange interaction across the boundary of the sublattices, Fe(4)-O(2)-Fe(5), can be affected by a proper substitution, e.g., replacing the large Ba^{2+} with the smaller Sr^{2+} [18]. Therefore, the T block, which contains the Fe(4)-O(2)-Fe(5) bonds, is essential in bringing into being the non-collinear screw structure in the Y-type hexaferrite. The Y-type hexagonal ferrite $Ba_{0.5}Sr_{1.5}Zn_2Fe_{12}O_{22}$ is a multiferroic material at room temperature in a low magnetic field of 0.1 T. The magnetic phase transitions in single crystal $Ba_{0.5}Sr_{1.5}Zn_2Fe_{12}O_{22}$ hexaferrites have been studied thoroughly, with the magnetic-phase diagram data exhibiting significant complexity [19,20]. Of importance were found to be not only the crystallographic positions occupied by metal cations, but also the defects in the crystal lattice, including those of oxygen at the crystal surface. Generally, two transitions are taking place – from collinear ferromagnetic to proper-screw (helical)

Published in : Journal of Magnetism and Magnetic Materials (2020), vol. 505, 166725
DOI:10.1016/j.jmmm.2020.166725
Status : Postprint (Author's version)

spin order, and from proper-screw to conical spin order. It was also found that $Ba_{0.5}Sr_{1.5}Zn_2Fe_{12}O_{22}$ shows a helical spin order, where the spin moments lie and rotate in the *ab*-plane below 326 K (Néel temperature) [20]. The partial substitution of Ba^{2+} cations with Sr^{2+} cations in $Ba_{2-x}Sr_xZn_2Fe_{12}O_{22}$ leads to a lattice deformation around the Sr^{2+} positions due to the smaller ionic radius of strontium accompanied with a redistribution of Zn^{2+} and Fe^{3+} in the tetrahedral sites. Lately, single crystals of $Ba_{0.5}Sr_{1.5}Ni_2Fe_{12}O_{22}$ were reported to order magnetically at much higher temperatures (T_N = 650 K) than $Ba_{0.5}Sr_{1.5}Zn_2Fe_{12}O_{22}$ (T_N = 326 K) [6,20].

Therefore, motivated by the wide range of applications and unique magnetic properties of the hexaferrites in powder form, an attempt was made in the present work to understand the effect of the magnetic cation (Ni^{2+}) substitution for the diamagnetic Zn^{2+} on the magnetic phase transition of $Ba_{0.5}Sr_{1.5}Zn_{2-x}Ni_xFe_{12}O_{22}$ (x = 0.8, 1, 1.5) powders.

2. Experimental

Polycrystalline samples of Ni-doped $Ba_{0.5}Sr_{1.5}Zn_2Fe_{12}O_{22}$ were fabricated by a modified citric acid sol–gel auto-combustion using stoichiometric amounts of the precursors. The corresponding metal nitrates were used as starting materials, and a citric acid solution was slowly added to the mixed nitrates as a chelator to form stable complexes with the metal cations. The solution was then slowly evaporated to form a gel, which was dehydrated at 120 °C and turned into a fluffy mass which burned in a self-propagating combustion manner. The auto-combusted powders obtained were homogenized and thermally treated using an STF 15/450 Carbolite furnace as follows: heating up to 800 °C at a heating rate of 200 °C/h; the material was then kept at 800 °C for three hours to remove any remaining organic components; finally, the powder was cooled slowly to room temperature at the average cooling rate of 70 °C/h. Then the powders were pressed at 7 MPa to bulk pellets with a diameter of 16 mm. The pressing mold was treated with paraffin viscous (Merck) and no binder was used. The pellets were annealed at 1170 °C in air for 10 h after heating at the maximal furnace heating rate to obtain the $Ba_{0.5}Sr_{1.5}Zn_{2-x}Ni_xFe_{12}O_{22}$ compositions with x = 0.8, 1, and 1.5. Finally, the pellets were cooled down freely to room temperature at the average cooling rate of 70 °C/h. The bulk material thus obtained is suitable for microscopic studies of the effect of Ni substitution on the morphology of $Ba_{0.5}Sr_{1.5}Zn_{2-x}Ni_xFe_{12}O_{22}$ particles. The pellets were cut to study their homogeneity by microscopic and EDS analyses. Finally, the pellets were ground to obtain the powder materials for magnetic measurements.

The structure and phase purity of the sintered pellets were investigated by X-ray diffraction (XRD) measurements performed using a Brucker D8 diffractometer (40 kV, 30 mA) controlled by a DIFFRACT-PLUS software in Bragg-Brentano reflection geometry with Cu-Kα radiation (λ = 1.5418 Å). Scanning electron microscopy and energy dispersive X-ray spectroscopy (FEI XL30 FEG-ESEM, Bruker Quantax EDS coupled to ESEM) were used to determine the samples' morphology and the Ba:Sr:Zn:Ni:Fe ratio, respectively. The magnetic properties were measured by means of a physical-property-measurement-system (PPMS) from Quantum Design equipped with an ACMS option. The hysteresis measurements were conducted at 4.2 K. The *ac* susceptibility was measured in an *ac*

Published in : Journal of Magnetism and Magnetic Materials (2020), vol. 505, 166725
DOI:10.1016/j.jmmm.2020.166725
Status : Postprint (Author's version)

magnetic field with amplitude of 10 Oe at a frequency of 1 kHz. The sample was first cooled down to 4.2 K in the absence of a magnetic field and the *ac* susceptibility was measured as the temperature was raised up to 300 K.

3. Results and discussion

Fig. 1 (a) and **(b)** show typical X-ray diffraction patterns of the as-obtained auto-combusted powder and of the powder thermally-treated at 800 °C for three hours. For all compositions, the as-synthesized samples consisted of a spinel-type phase with crystallite sizes in the range 10–12 nm and a unit cell parameter around 8.37–8.375 Å. The latter value is intermediate between that of $NiFe_2O_4$ (8.336 Å) and that of $ZnFe_2O_4$ (8.441 Å), suggesting a spinel structure of Ni - Zn mixed ferrite (Zn, Ni)Fe_2O_4. The second crystalline phase is a mixed carbonate of barium and strontium, i.e. (Ba, Sr)CO_3, as can be deduced from the intermediate cell parameters between those of $BaCO_3$ and of SrCO3. The crystallite size of this phase is about 18–19 nm. The thermal treatment of all compositions at 800 °C leads to the disappearance of the carbonate constituent and the formation of oxide products with the participation of Ba and Sr, namely $BaFeO_{3-x}$ and $BaSrFe_4O_8$. The amount of hexagonal $BaSrFe_4O_8$ is higher for samples with a Zn:Ni ratio other than 1. More information is given in the supplementary file. The powders obtained after thermal treatment at 800 °C were used for pellet preparation and were further synthesized at 1170° C in air for ten hours.

As can be seen in the XRD patterns, none of the substances in the auto-combusted powder and the one thermally-treated at 800 °C were observed as second phases in the obtained $Ba_{0.5}Sr_{1.5}Zn_{2-x}Ni_xFe_{12}O_{22}$ (x = 0.8, 1, and 1.5) (**Fig. 1** c, d, e). In our synthesis, there were no signs of nickel spinel ferrite decomposition to NiO as observed by Corso et al. [21]. More information is given in the supplementary file.

The calculated crystal cell parameters a and c are presented in **Table 1**. The X-ray density ($D_{X\text{-}ray}$) of the samples is calculated from the XRD data, while the experimental density (D_{ex}) is calculated from the samples' mass and size [22]. As can be seen, the presence of Ni^{2+} cations did not alter significantly the crystal cell parameters. There is no difference in the calculated values of X-ray density due to the similar crystal cell parameters of the three samples. As expected, the values of the experimental density are lower than those of the X-ray density, in line with our intent to achieve sufficient inter-particle distance to study the samples' morphology.

Fig. 2 shows SEM images of polished cross-sections of the bulk samples. As can be seen, the Ni substitution did not affect the samples' microstructure. For each sample, energy-dispersive X-ray (EDS) microanalysis was performed on the shown area and four separate points of **Fig. 2**; the averaged results for the elemental ratios, together with the unit cell parameters are summarized in **Table 1**. As can be seen, the Ba:Sr:Zn:Ni:Fe ratio corresponds to the stoichiometric one.

Published in : Journal of Magnetism and Magnetic Materials (2020), vol. 505, 166725
DOI:10.1016/j.jmmm.2020.166725
Status : Postprint (Author's version)

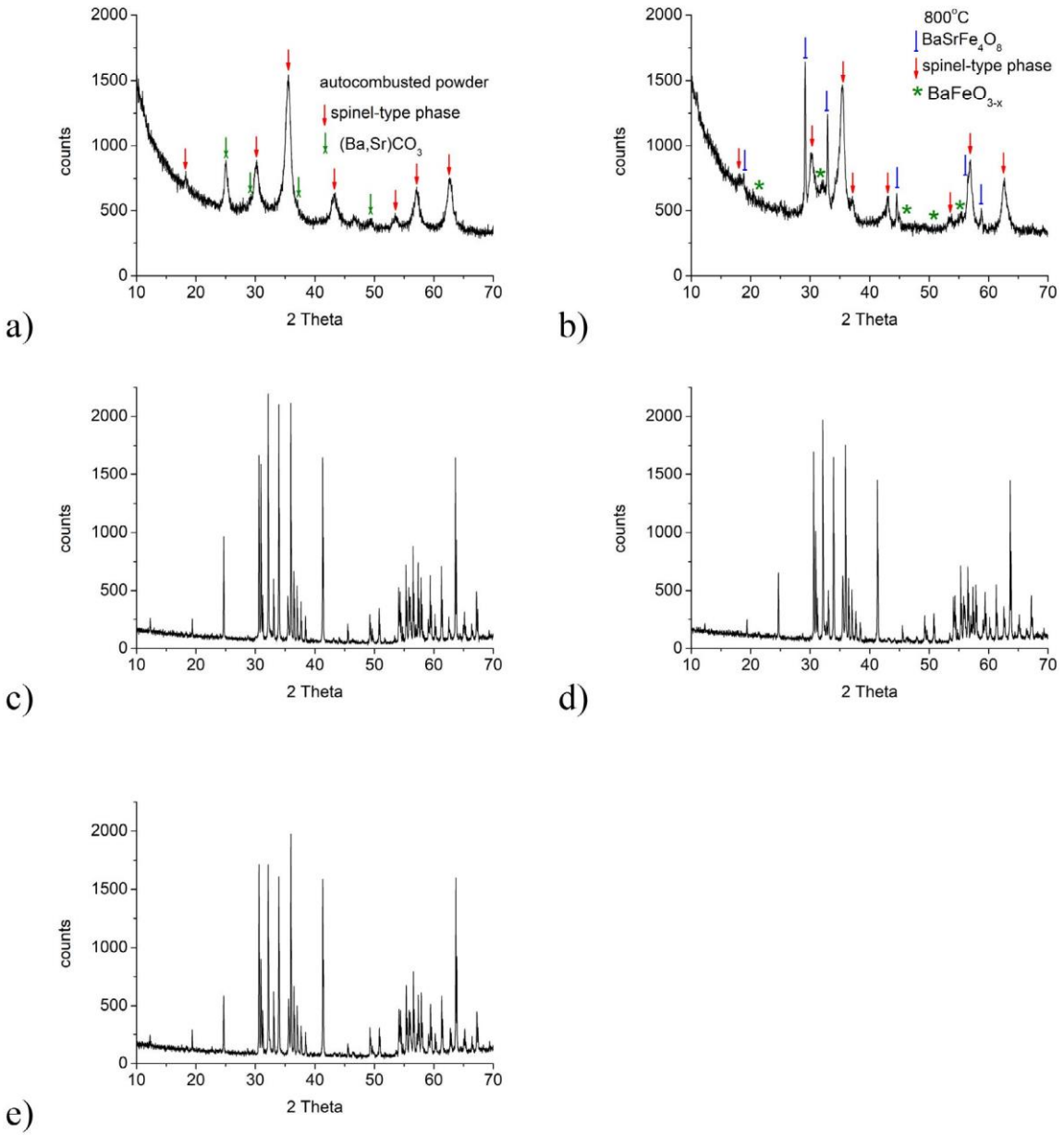

Fig. 1. XRD patterns of (a) auto-combusted powder, (b) powder annealed at 800 °C for 3 h (c) $Ba_{0.5}Sr_{1.5}Zn_{1.2}Ni_{0.8}Fe_{12}O_{22}$, (d) $Ba_{0.5}Sr_{1.5}ZnNiFe_{12}O_{22}$ and (e) $Ba_{0.5}Sr_{1.5}Zn_{0.5}Ni_{1.5}Fe_{12}O_{22}$.

Table 1. Unit cell parameters *a*, *c*, experimental D_{exp} and calculated X-ray density $D_{X\text{-}ray}$, and Ba:Sr:Zn:Ni:Fe ratio from EDS analysis of $Ba_{0.5}Sr_{1.5}Zn_{2-x}Ni_xFe_{12}O_{22}$ (x = 0.8, 1, 1.5) samples.

Sample	*a*, Å	c, Å	$D_{X\text{-}ray}$, g/cm^3	D_{exp}, g/cm^3	Ba:Sr:Zn:Ni:Fe
$Ba_{0.5}Sr_{1.5}Zn_{1.2}Ni_{0.8}Fe_{12}O_{22}$	5.915	40.743	5.455	3.104	0.5:1.5:1.1:0.8:12:1
$Ba_{0.5}Sr_{1.5}ZnNiFe_{12}O_{22}$	5.914	40.748	5.453	3.784	0.5:1.6:1.1:1:12.3
$Ba_{0.5}Sr_{1.5}Zn_{0.5}Ni_{1.5}Fe_{12}O_{22}$	5.911	40.743	5.456	3.565	0.5:1.5:0.5:1.47:12.2

Published in : Journal of Magnetism and Magnetic Materials (2020), vol. 505, 166725
DOI:10.1016/j.jmmm.2020.166725
Status : Postprint (Author's version)

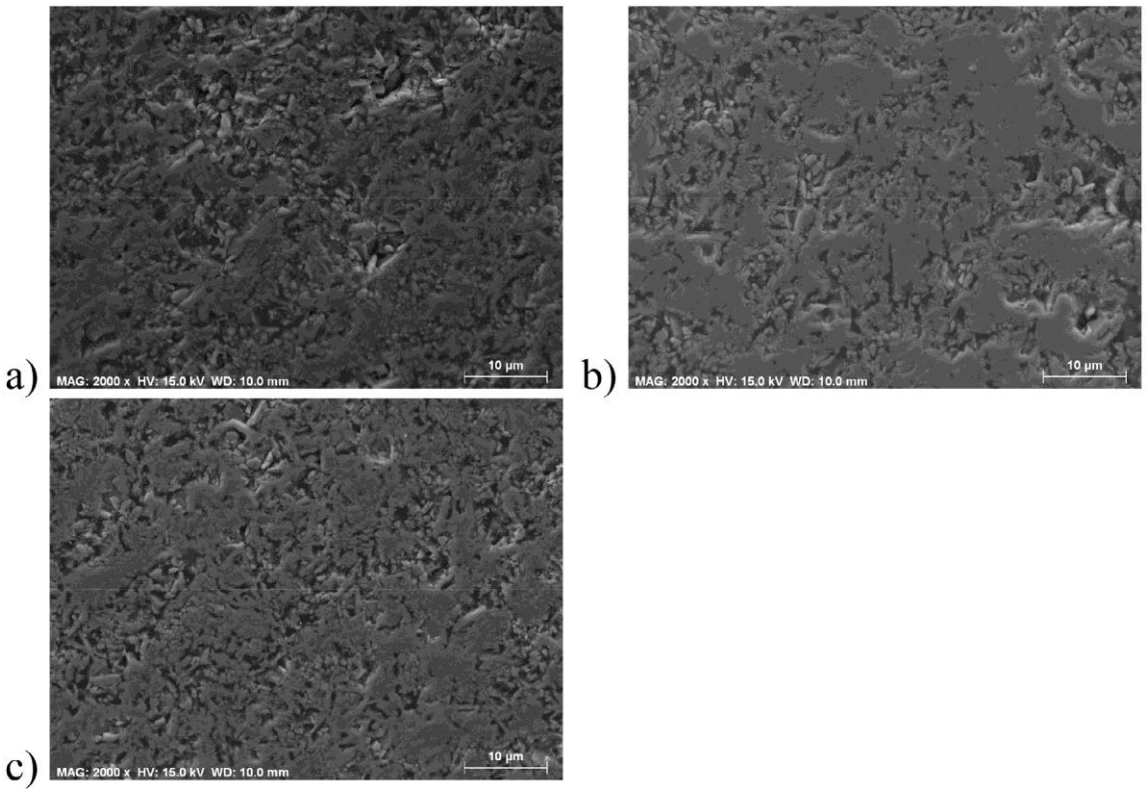

Fig. 2. SEM images of (a) $Ba_{0.5}Sr_{1.5}Zn_{1.2}Ni_{0.8}Fe_{12}O_{22}$, (b) $Ba_{0.5}Sr_{1.5}ZnNiFe_{12}O_{22}$ and (c) $Ba_{0.5}Sr_{1.5}Zn_{0.5}Ni_{1.5}Fe_{12}O_{22}$.

Fig. 3 presents the differential susceptibility of $Ba_{0.5}Sr_{1.5}Zn_{2-x}Ni_xFe_{12}O_{22}$ (x = 0.8, 1, 1.5) in the temperature region 4–300 K. The real part of the *ac* susceptibility increases with the temperature; a change in its behavior is seen at a temperature of about 225 K, namely, a sharp rise. It should be emphasized that, in contrast with the other two samples, for the composition x = 0.8 no maximum of the real part curve is observed at 300 K; and neither is a maximum present in its imaginary part curve at about 280–290 K. This indicates that the helicoidal/ferromagnetic transition occurs above room temperature. Two maxima are seen in the imaginary part of ac-susceptibility curves at 10 K and 148 K. We relate the maximum at 148 K to the magnetic-phase transition from conical spin order to hellicoidal spin order. In the sample x = 1, in which the ratio between Zn and Ni is 1, there is a weakly expressed maximum in the imaginary part of ac-susceptibility curve at 177 K and a maximum at 282 K due to the magnetic phase transitions from conical spin order to hellicoidal spin and from helicoidal to ferrimagnetic spin order, respectively. At the highest substitution level (x = 1.5), there is only one maximum in the imaginary part of ac-susceptibility curves at 284 K, which we believe is due to a magnetic phase transition from helicoidal to ferrimagnetic spin order.

To investigate the magnetic behavior at low temperatures, we measured the magnetization in an applied magnetic field at 4.2 K (**Fig. 4**). The magnetization curves of compositions x = 0.8 and 1 show a similar course. The magnetization steeply increases up to H ~ 1.7 kOe and then exhibits a different behavior – a divergent tendency up to H ~ 30 kOe. Similar behavior has been reported by

Published in : Journal of Magnetism and Magnetic Materials (2020), vol. 505, 166725
DOI:10.1016/j.jmmm.2020.166725
Status : Postprint (Author's version)

Hiraoka et al. [23] for a $Ba_{0.5}Sr_{1.5}Ni_2Fe_{12}O_{22}$ single crystal at 20 K, providing evidence for magnetic-field-induced transitions between different magnetic arrangements. One can see that in the $Ba_{2-x}Sr_xZn_2Fe_{12}O_{22}$ system, the case $x = 1$ exhibits the highest saturation magnetization value. The most likely cause is the cationic distribution in the sublattices in a way that results in the highest net magnetization of the sample.

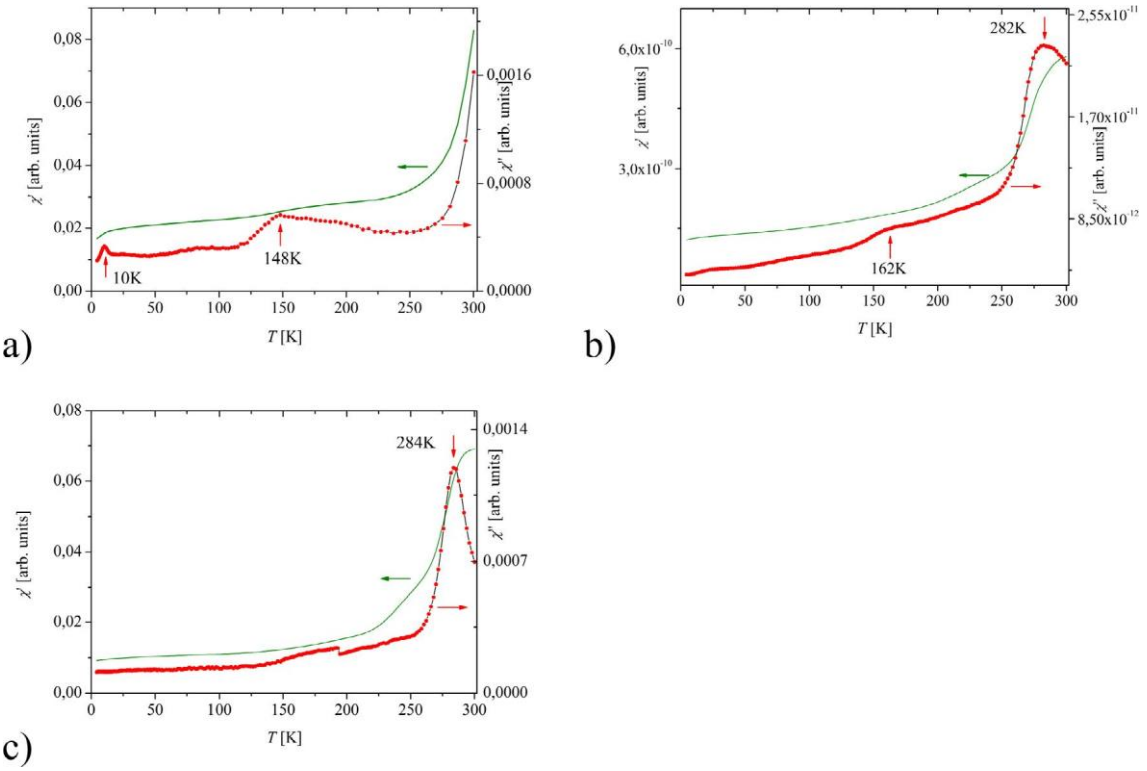

Fig. 3. Temperature dependence of the differential *ac* susceptibility (real part 𝜒', and imaginary part 𝜒'') of the compositions (a) $Ba_{0.5}Sr_{1.5}Zn_{1.2}Ni_{0.8}Fe_{12}O_{22}$, (b) $Ba_{0.5}Sr_{1.5}ZnNiFe_{12}O_{22}$ and (c) $Ba_{0.5}Sr_{1.5}Zn_{0.5}Ni_{1.5}Fe_{12}O_{22}$ recorded at an *ac*-magnetic field with an amplitude of 10 Oe and a frequency of 1000 Hz.

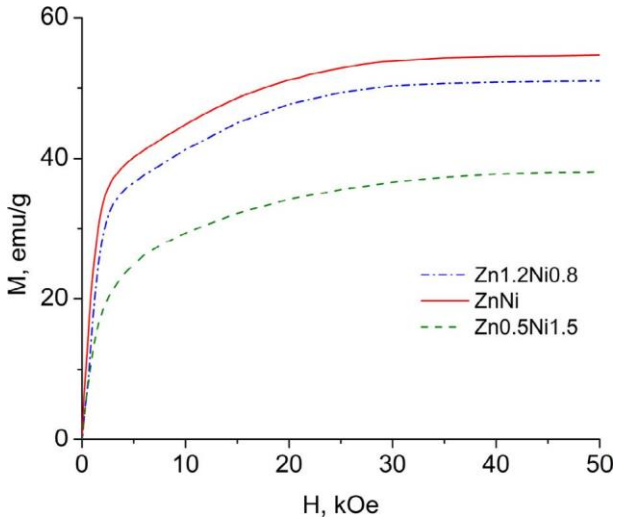

Fig. 4. Initial magnetization of $Ba_{0.5}Sr_{1.5}Zn_{2-x}Ni_xFe_{12}O_{22}$ ($x = 0.8, 1, 1.5$) at 4.2 K.

Published in : Journal of Magnetism and Magnetic Materials (2020), vol. 505, 166725
DOI:10.1016/j.jmmm.2020.166725
Status : Postprint (Author's version)

It is noteworthy that the sample with the highest content of nickel ions, which bear magnetic moments, has a lower value of magnetization of 5 kOe than the other two samples. This should be related to the known preference of the non-magnetic Zn^{2+} cations to occupy tetrahedral positions, whereas magnetic Ni^{2+} cations prefer to enter octahedral positions [24]. This entails the migration of iron cations between crystallographic sites with octahedral and tetrahedral oxygen configuration and is accompanied by a corresponding change in the magnetic structure.

Fig. 5 presents the hysteresis curves of the investigated compositions. As can be seen from their course in the low magnetic field region (right panel), a triple hysteresis loop is evident to occur for all three compositions, which points to the presence of two kinds of ferromagnetic states with different magnetization values. It is well known that in $Ba_{2-x}Sr_xZn_2Fe_{12}O_{22}$ the substitution of Sr^{2+} at x = 1.5 results in a change in the magnetic phase from the ferromagnetic arrangement of Fe^{3+} spins in unsubstituted samples to a screw spin order. Once affected by a magnetic field, in the region of a low magnetic field the magnetic system undergoes transitions through metamagnetic states, including those between screw spin order and conical spin order. The change in the magnetic structure affects the magnetization of the specimen and gives rise to the observation of a multistage hysteresis loop. Similar behavior with a triple hysteresis loop is shown by Khanduri et al. [25] for $Ba_{2-x}Sr_xMg_2Fe_{12}O_{22}$. In our study, this behavior is best expressed by the composition $Ba_{0.5}Sr_{1.5}ZnNiFe_{12}O_{22}$. More detailed studies using neutron diffraction are needed to unravel the magnetic structure of the intermediate phases and the distribution of magnetic cations (Fe^{3+}, Ni^{2+}).

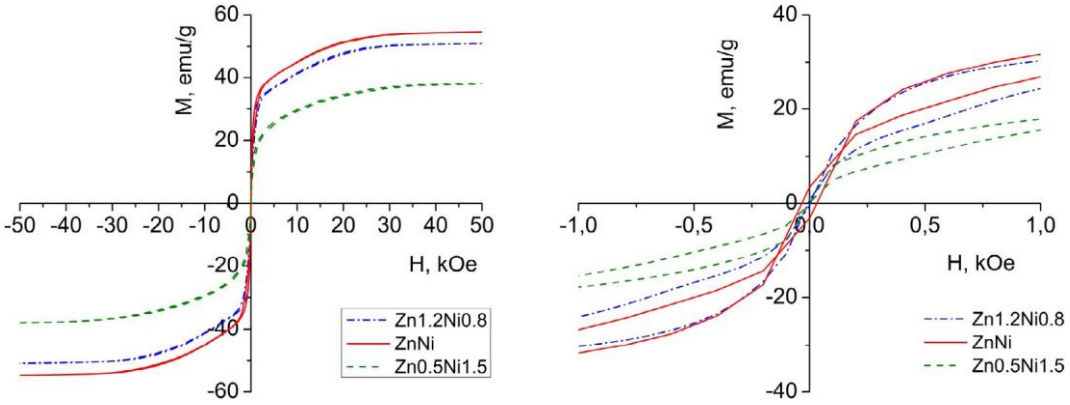

Fig. 5. Hysteresis curves of $Ba_{0.5}Sr_{1.5}Zn_{2-x}Ni_xFe_{12}O_{22}$ (x = 0.8, 1, 1.5) at 4.2 K. The right panel shows the course of magnetization in the low magnetic field region.

4. Conclusion

The structural and magnetic properties of three different compositions of the Y-type hexaferrite system $Ba_{0.5}Sr_{1.5}Zn_{2-x}Ni_xFe_{12}O_{22}$ (x = 0.8, 1, 1.5) were investigated by X ray diffraction, scanning electron microscopy, energy dispersive X-ray spectroscopy and static and dynamic magnetization measurements. The samples were prepared by following a modified citric acid self-combustion route providing products with an atomic ratio of the elements that is characteristic of the

Published in : Journal of Magnetism and Magnetic Materials (2020), vol. 505, 166725
DOI:10.1016/j.jmmm.2020.166725
Status : Postprint (Author's version)

stoichiometric composition and a microstructure and crystallinity practically unaffected from the nickel substitution level. The magnetization and *ac* susceptibility showed a rather complicated behavior manifested by specific triple magnetic hysteresis loops for the three studied compositions and reflected in the magnetic field-induced transitions between the magnetic arrangements depending on the degree of nickel substitution. We observed an increase in the temperature of the magnetic phase transitions as the amount of Ni replacing Zn is increased. In this way, we obtained a material that is promising for a variety of applications (for example, nonvolatile memory) based on the properties of a single-phase multiferroic at room temperature.

Declaration of Competing Interest

The authors declare that they have no known competing financial interests or personal relationships that could have appeared to influence the work reported in this paper.

Acknowledgments

The work was supported in part by the Bulgarian National Science Fund, Bulgaria, under contract DN 08/4 "Novel functional ferrites-based magneto-electric structures"; by a joint research project "Studies of the structural and microwave properties of magnetic nanocomposites for microwave absorption applications" between the Bulgarian Academy of Sciences, Bulgaria and WBI, Belgium; and by a joint research project "Investigation of structural and magnetic phase transitions in multifunctional materials – oxides and alloys with applications in electronics and medicine" between the Bulgarian Academy of Sciences, Bulgaria and the Institute of Low Temperature and Structure Research, Polish Academy of Sciences, Poland. B. Georgieva was supported for the synthesis and structural properties by the Bulgarian Ministry of Education and Science, Bulgaria under the National Research Program "Young scientists and postdoctoral students" approved by DCM # 577/17.08.2018.

Appendix A. Supplementary data

Supplementary data to this article can be found online at

https://doi.org/10.1016/j.jmmm.2020.166725.

Published in : Journal of Magnetism and Magnetic Materials (2020), vol. 505, 166725
DOI:10.1016/j.jmmm.2020.166725
Status : Postprint (Author's version)

References

[1] J. Hemberger, P. Lunkenheimer, R. Fichtl, H.-A. Krug von Nidda, V. Tsurkan, A. Loidl, Relaxor ferroelectricity and colossal magnetocapacitive coupling in ferromagnetic $CdCr_2S_4$, Nature 434 (2005) 364–367, https://doi.org/10.1038/ nature03348.

[2] T. Kimura, Magnetoelectric hexaferrites, Annu. Rev. Condens. Matter Phys. 3 (2012) 93–110, https://doi.org/10.1146/annurev-conmatphys-020911-125101.

[3] Y. Tokura, S. Seki, Multiferroics with spiral spin orders, Adv Mater. 22 (2010) 1554–1556, https://doi.org/10.1002/adma.200901961.

[4] S.-W. Cheong, M. Mostovoy, Multiferroics: a magnetic twist for ferroelectricity, Nat. Mater. 6 (2007) 13–20, https://doi.org/10.1038/nmat1804.

[5] M. Gich, I. Fina, A. Morelli, F. Sánchez, M. Alexe, J. Gàzquez, J. Fontcuberta, A. Roig, Multiferroic iron oxide thin films at room temperature, Adv. Mater. 26 (2014) 4645–4652, https://doi.org/10.1002/adma.201400990.

[6] T. Kimura, G. Lawes, A.P. Ramirez, Electric polarization rotation in a hexaferrite with long-wavelength magnetic structures, Phys. Rev. Lett. 94 (2005) 137201, https://doi.org/10.1103/PhysRevLett.94.137201.

[7] Sh. Ishiwata, Y. Taguchi, H. Murakawa, Y. Onose, Y. Tokura, Low-magnetic-field control of electric polarization vector in a helimagnet, Science 319 (2008) 1643–1646, https://doi.org/10.1126/science.1154507.

[8] S. Shen, Y. Chai, Y. Sun, Nonvolatile electric-field control of magnetization in a Y-type Hexaferrite, Sci. Rep. 5 (2015) 8254, https://doi.org/10.1038/srep08254.

[9] S.H. Chun, Y.Sh. Chai, B.-G. Jeon, H.J. Kim, Y.S. Oh, I. Kim, H. Kim, B.J. Jeon, S.Y. Haam, J.-Y. Park, S.H. Lee, J.-H. Chung, J.-H. Park, K.H. Kim, Electric field control of nonvolatile four-state magnetization at room temperature, Phys. Rev. Lett. 108 (2012) 177201, https://doi.org/10.1103/PhysRevLett.108.177201.

[10] Y.S. Chai, S. Kwon, S.H. Chun, I. Kim, B.-G. Jeon, K.H. Kim, S. Lee, Electrical control of large magnetization reversal in a helimagnet, Nature Comm. 5 (2014) 4208, https://doi.org/10.1038/ncomms5208.

[11] K. Okumura, K. Haruki, T. Ishikura, S. Hirose, T. Kimura, Multilevel magnetization switching by electric field in c-axis oriented polycrystalline Z-type hexaferrite, Appl. Phys. Lett. 103 (2013) 032906, https://doi.org/10.1063/1.4816268.

[12] S. Hirose, K. Haruki, A. Ando, T. Kimura, Mutual control of magnetization and electrical polarization by electric and magnetic fields at room temperature in Y-type $BaSrCo_{2-x}Zn_xFe_{11}AlO_{22}$ ceramics, Appl. Phys. Lett. 104 (2014) 022907, https:// doi.org/10.1063/1.4862432.

[13] R.C. Pullar, Hexagonal ferrites: a review of the synthesis, properties and applications of hexaferrite ceramics, Prog. Mater. Sci. 57 (2012) 1191–1334. https://doi. org/10.1016/j.pmatsci.2012.04.001.

[14] K. Kouřil, V. Chlan, H. Štěpánková, P. Novák, K. Knížek, J. Hybler, T. Kimura, Y. Hiraoka, J. Buršík, Hyperfine interactions in magnetoelectric hexaferrite system, J. Magn. Magn. Mater. 322 (2010) 1243–1245, https://doi.org/10.1016/j.jmmm. 2009.03.011.

[15] K. Kouřil, V. Chlan, H. Štěpánková, A. Telfah, P. Novák, K. Knížek, Y. Hiraoka, T. Kimura, Distribution of Zn in magnetoelectric Y-type hexaferrite, Acta Phys. Pol. A 118 (2010) 732–733.

[16] E.W. Gorter, Saturation magnetization of some ferrimagnetic oxides with hexagonal crystal structures, Proc. IEE - Part B: Radio and Electron. Eng. 104 (1957) 255–260, https://doi.org/10.1049/pi-b-1.1957.0042.

[17] K. Taniguchi, N. Abe, S. Ohtani, H. Umetsu, T. Arima, Ferroelectric polarization reversal by a magnetic field in multiferroic Y-type hexaferrite $Ba_2Mg_2Fe_{12}O_{22}$, Appl. Phys. Express 1 (2008) 031301, https://doi.org/10.1143/APEX.1.031301.

[18] E. Pollert, Crystal chemistry of magnetic oxides part 2: Hexagonal ferrites, Prog. Cryst. Growth Charact. 11 (1985) 155–205, https://doi.org/10.1016/0146-3535(85)90033-4.

[19] N. Momozawa, Y. Yamaguchi, H. Takei, M. Mita, Magnetic structure of $(Ba_{1-x}Sr_x)$ $2Zn_2Fe_{12}O_{22}$ (x = 0-1.0), J. Phys. Soc. Jap. 54 (1985) 771–780. https://doi.org/ 10.1143/JPSJ.54.771.

[20] Y.S. Chai, S.H. Chun, S.Y. Haam, Y.S. Oh, I. Kim, K.H. Kim, Low-magnetic-field control of dielectric constant at room temperature realized in $Ba_{0.5}Sr_{1.5}Zn_2Fe_{12}O_{22}$, New J. Phys. 11 (2009) 073030, https://doi.org/10.1088/1367-2630/11/7/ 073030.

[21] S. Corso, Ph. Tailhades, I. Pasquet, A. Rousset, V. Laurent, A. Gabriel, C. Condolf, Preparation conditions of pure and stoichiometric $Ni_xFe_{3-x}O_4$ bulk ceramics, Solid State Sci. 6 (2004) 791–798, https://doi.org/10.1016/j.solidstatesciences.2004.03. 037.

[22] V.V. Warhate, D.S. Badwaik, Structural, magnetic and thermomagnetic properties of strontium NiMn Y-Type nano-hexaferrite, J. Alloy. Comp. 818 (2020) 152830, https://doi.org/10.1016/j.jallcom.2019.152830.

[23] Y. Hiraoka, H. Nakamura, M. Soda, Y. Wakabayashi, T. Kimura, Magnetic and magnetoelectric properties of $Ba_{2-x}Sr_xNi_2Fe_{12}O_{22}$ single crystals with Y-type hexaferrite structure, J. Appl. Phys. 110 (2011) 033920, https://doi.org/10.1063/1. 3622332.

[24] M.A. El Hiti, A.M. Abo El Ata, Semiconductivity in $Ba_2Ni_{2-x}Zn_xFe_{12}O_{22}$ Y-type hexaferrites, J. Magn. Magn. Mater. 195 (1999) 667–678, https://doi.org/10.1016/ S0304-8853(99)00120-1.

[25] H. Khanduri, M. Chandra Dimri, H. Kooskora, I. Heinmaa, G. Viola, H. Ning, M.J. Reece, J. Krustok, R. Stern, Structural, dielectric, magnetic, and nuclear magnetic resonance studies of multiferroic Y-type hexaferrites, J. Appl. Phys. 112 (2012) 073903, https://doi.org/10.1063/1.4754532.